Atmospheric
Chemistry
and Physics

Laser filament-induced aerosol formation

H. Saathoff[1], S. Henin[2], K. Stelmaszczyk[3], M. Petrarca[2], R. Delagrange[2], Z. Hao[3], J. Lüder[3], O. Möhler[1], Y. Petit[2], P. Rohwetter[3], M. Schnaiter[1], J. Kasparian[2], T. Leisner[1], J.-P. Wolf[2], and L. Wöste[3]

[1]Karlsruhe Institute of Technology, Institute for Meteorology and Climate Research, Hermann-von-Helmholtz-Platz 1, 76344 Eggenstein-Leopoldshafen, Germany
[2]GAP, Université de Genève, Chemin de Pinchat 22, 1211 Genève 4, Switzerland
[3]Institut für Experimentalphysik, Freie Universität Berlin, Arnimallee 14, 14195 Berlin, Germany

Correspondence to: J. Kasparian (jerome.kasparian@unige.ch)

Abstract. Using the aerosol and cloud simulation chamber AIDA, we investigated the laser filament induced particle formation in ambient air, humid synthetic air, humid nitrogen, argon–oxygen mixture, and pure argon in order to simulate the particle formation under realistic atmospheric conditions as well as to investigate the influence of typical gas-phase atmospheric constituents on the particle formation. Terawatt laser plasma filaments generated new particles in the size range 3 to 130 nm with particle production rates ranging from 1×10^7 to 5×10^9 cm^{-3} plasma s^{-1} for the given experimental conditions. In all cases the particle formation rates increased exponentially with the water content of the gas mixture. Furthermore, the presence of a few ppb of trace gases like SO_2 and α-pinene clearly enhanced the particle yield by number, the latter also by mass. Our findings suggest that new particle formation is efficiently supported by oxidized species like acids generated by the photoionization of both major and minor components of the air, including N_2, NH_3, SO_2 and organics.

1 Introduction

In recent years femtosecond laser pulses fired into the atmosphere have shown to generate self-guided filaments (Kasparian et al., 2003; Couairon and Mysyrowicz, 2007; Bergé et al., 2007; Kasparian and Wolf, 2008; Chin et al., 2005) in a dynamic balance between Kerr self-focusing and defocusing by the self-generated plasma and/or negative higher order Kerr terms (Béjot et al., 2010). They can deliver an intensity as high as 5×10^{13} W cm^{-2} at kilometer-range distances (Rodriguez et al., 2004), sufficient for ionizing and photoox-

idizing the air (Petit et al., 2010), allowing a very rich plasma chemistry implying both neutral and ionized species (Kossyi et al., 1992; Xu et al., 2009; Dotan et al., 1997; Bardsley, 1968; Braginskiy et al., 2005).

Filaments generated by ultrashort laser pulses were recently proposed as candidates to promote condensation of water in the atmosphere (Rohwetter et al., 2010) or generate snow (Ju et al., 2012). However, so far only little information on the laser-induced particle formation, potential growth of these particles, and the corresponding uptake of water on these particles is available (Rohwetter et al., 2011). It was shown, in particular, that uptake of water on laser-induced particles is assisted by laser-generated hygroscopic HNO_3 (Petit et al., 2010; Rohwetter et al., 2011), generated in the plasma trail left behind by the laser filaments. Similar results have also been reported for illumination with ultraviolet light (Yoshihara, 2005; Sorokin and Arnold, 2009; Sorokin, 2010). No data have been however available to date on the laser filament capability of nucleating new particles from the gas phase.

Therefore, this work aims at systematically studying the laser filament-induced particle formation in humid inert gases, in humid air, and in ambient air under well-controlled conditions with extremely low background particle concentration. The experiments were performed in the large-scale aerosol and cloud chamber AIDA (Aerosol Interaction and Dynamics in the Atmosphere) (Möhler et al., 2003; Schnaiter et al., 2012) under illumination by the TW-class mobile laser system *Teramobile* (Wille et al., 2002). Temperature, relative humidity, trace gas levels, and laser power were varied systematically.
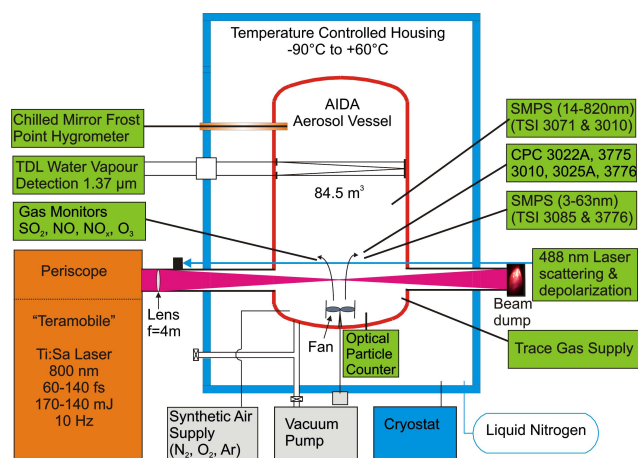
Fig. 1. Schematic of the experimental set-up of the *Teramobile* laser system at the AIDA aerosol and cloud chamber. The terawatt laser beam (red line) is generated in a container outside the AIDA hall and directed via transfer optics, a focussing lens (f = 4 m), and an entrance window (139 mm diameter, 9.8 mm thickness) across the AIDA vessel and the air flux from its mixing fan. The beam exits at opposite side through an exit window into a beam dump. Sampling tubes for particles and trace gases are shown as black lines. The light blue line represents the 488 nm laser beam used for in situ light scattering measurements.

2 Experimental set-up

As sketched in Fig. 1, the aerosol and cloud chamber AIDA features 4 m diameter and 7.5 m height (84.5 m^3) (Möhler et al., 2003; Schnaiter et al., 2012). The beam of the Teramobile mobile femtosecond terawatt laser system (Wille et al., 2002) was expanded to 10 cm diameter and focused by an f = 4 m lens into the centre of the AIDA chamber. We used laser pulses at a central wavelength of 800 nm and a repetition rate of 10 Hz. In two sets of experiments, the pulse energy and duration were ∼ 140 mJ, 140 fs ("weak filamentation", generating ten filaments with 100 cm length each) and 170 mJ, 60 fs ("strong filamentation", 20 filaments, 50 cm length each), respectively. The filaments, of 100 µm diameter, covered a volume of typically 80 mm^3 (∼ 0.08 cm^3) in each case. Shot-to-shot laser pulse energy stability was 3 % RMS. Optionally, a mixing fan (31 m^3 min^{-1}) located about 10 cm below the laser beam homogenized the atmosphere inside the simulation chamber within 1–2 min, diluting the species produced in the filament volume by a factor of about 10^8.

Trace gases were sampled via Teflon tubes (FEP, 4 mm inner diameter) placed 5 cm away from the central AIDA axis and the laser beam, directly above the mixing fan. Aerosol particles were sampled through stainless steel tubes located ∼ 15 cm above the laser beam and 60 cm away from the central axis of the AIDA chamber, towards the laser exit window. Cloud droplets were sampled via vertical stainless steel tubes in the bottom of the AIDA chamber.

Experiments have been performed within temperature and relative humidity (RH) ranges of 245–283 K and 25–98 %, respectively (cf. Table 1). Before each experiment the AIDA chamber was evacuated to about 1 Pa of total pressure and flushed several times with synthetic air. Then the desired amount of water vapour was evaporated into the evacuated chamber from a stainless steel reservoir containing purified water (Nanopure, Barnstead) at 30 °C, and the chamber was then filled to atmospheric pressure with synthetic air (99.9990 %, hydrocarbons < 0.5 ppmv, Basi). The atmospheric pressure ranged between 998 and 1016 hPa for the experiments presented in this work. The remaining background particle concentration was 0.1–1 cm^{-3}. Alternatively, argon (99.9990 %, hydrocarbons < 0.1 ppmv, Air Liquide), nitrogen (99.9990 %, hydrocarbons < 0.2 ppmv, Air Liquide), oxygen (99.998 %, hydrocarbons < 0.2 ppmv, Air Liquide), or ambient air passed through a PM$_{10}$ inlet (DPM10/2,3/01, Digitel) to remove particles larger than 10 µm was used instead of synthetic air. The ambient air filled into the simulation chamber was sampled about 10 m above ground level on the roof of the AIDA building at KIT campus north near Eggenstein-Leopoldshafen, Germany (latitude: 49.09527° N, longitude: 8.42938° E; 112 m above sea level). Times are given in local time (Central European Summer Time, CEST). Trace gases like SO$_2$ (1 % SO$_2$ (99.98 %) in nitrogen, Linde) and NH$_3$ (3 % NH$_3$ (99.995 %) in nitrogen, Linde) were added to the simulation chamber from gas cylinders via a gas handling system with mass flow controllers. Toluene (99 %, Merck) and α-pinene (99 %, Aldrich) were added by evaporation of a well-defined pressure into a 1 L glass bulb and subsequent flushing into the AIDA chamber with a flow of 10 L min^{-1} synthetic air. Ammonium sulfate aerosol was generated with an atomizer (TSI 3076) from an aqueous solution of 1 wt% in water and added to the AIDA chamber via a diffusion dryer.

Ozone was measured with 20 s temporal resolution and a detection limit of 1 ppb (O341M, Environment SA). SO$_2$ was measured with 20 s temporal resolution and a detection limit of 1 ppb (AF22M, Environment SA). NO and NO$_x$ were measured with 30 s time resolution and a detection limit of 2 ppb (APNA-300E, Horiba). Water vapour was measured in situ by TDL (tunable diode laser) absorption spectroscopy with 1 s time resolution and a detection limit of about 100 ppb. In addition, the total water concentration was measured outside the chamber with a dew point mirror (373LX, MBW) sampling via a heated stainless steel tube.

The aerosol particle number concentration was measured with five different condensation particle counters (CPC 3010, 3022, 3775, 3025, 3776, TSI) for particles larger than 10, 7, 4, 3, and 2.5 nm, respectively, with a time resolution of 1 s. If not stated otherwise particle formation rates given in this paper are based on the particle number concentrations measured with the CPC 3025A or 3776 for particles larger than 3 or 2.5 nm, respectively. Aerosol particle size distributions were measured with two scanning mobility particle

Table 1. Experimental conditions for the experiments presented including typical particle production rates observed.

No.	T [K]	H_2O [%RH]	Main gases	Trace compounds	Particle production rate* [cm^{-3} plasma s^{-1}]	Fig.
1	283.6	64	100 % Ar	–	4×10^9	2, 3
2	283.6	55	85 % Ar, 15 % O_2	–	4×10^8	2, 3
3**	283.1	74	100 % N_2	–	(3×10^9)***	–
4	283.6	62(51)	79 % N_2, 21 % O_2	–	3.2×10^8 (1×10^7)	4, 5
5	283.6	97	79 % N_2, 21 % O_2	–	4.4×10^9	6, 7
6	283.6	60	79 % N_2, 21 % O_2	100 vppb NH_3	3.7×10^8	4, 5
7	283.6	58	79 % N_2, 21 % O_2	$1\,\mu g\,m^{-3}$ $(NH_4)_2SO_4$	1×10^9	4, 5
8	283.6	97	79 % N_2, 21 % O_2	60 ppb SO_2	2.4×10^9	6, 7
9	283.1	96	79 % N_2, 21 % O_2	–	8.0×10^7	8
10**	282.8	97	79 % N_2, 21 % O_2	–	1.4×10^8	8
11**	282.7	98	79 % N_2, 21 % O_2	–	8.0×10^7	8
12**	282.7	98	79 % N_2, 21 % O_2	–	7.1×10^7	8
13**	282.9	74	79 % N_2, 21 % O_2	–	1.5×10^7	8
14**	283.1	50	79 % N_2, 21 % O_2	–	1.4×10^7	8
15**	283.2	26	79 % N_2, 21 % O_2	–	1.1×10^7	8
16**	282.6	55	79 % N_2, 21 % O_2	–	1.0×10^7	8
17**	283.1	51	79 % N_2, 21 % O_2	15 ppb SO_2	1.8×10^9	–
18**	245.1	88	79 % N_2, 21 % O_2	22 ppb toluene	1.6×10^8	–
19**	283.0	92	79 % N_2, 21 % O_2	21 ppb α-pinene	3.6×10^8	9, 10
20**	283.0	90	79 % N_2, 21 % O_2	63 ppb α-pinene	1×10^9	9, 10
21**	283.0	89	79 % N_2, 21 % O_2	63ppb α-pinene, 7 ppb SO_2	4.8×10^9	9, 10
22	283.6	76	Ambient air	Particles, 15 ppb NO_x	1×10^9	11, 12
23	279.3	90	Ambient air		1×10^9	11, 12

* For particles larger than 2.5 or 3 nm. ** Results for weak filamentation. *** Number less precise due to higher particle background in the experiment.

sizers (SMPS, DMA 3071 with CPC 3010 & DMA 3085 with CPC 3776, TSI) with a time resolution of 300 s in the size ranges 14–820 nm and 3–63 nm, respectively. The temperature in both instruments was 296 K and both used dry sheath air. Particles in the size range 0.5–20 μm were measured with an aerodynamic particle sizer (APS 3321, TSI). Size distributions were described by their geometric mean diameter (GMD) and the geometric standard deviation (GSD) of the log-normal size distribution fitted to the measured one. In some experiments aerosol particles from the AIDA chamber were collected on 47 mm nylon membrane filters (Nylasorb, 1 μm, Gelman Science) for ion chromatographic analysis (DX500, Dionex) on soluble ions like sulfate and nitrate.

Effective particle formation rates per unit plasma filament volume (hereinafter denoted as cm^{-3} plasma s^{-1}) were calculated as the increase in measured particle number concentration (particles > 3 or 2.5 nm if not stated otherwise) during the laser firing period, divided by the time during which the laser was fired, and by the estimated plasma volume of $0.08\,cm^3$. This effective particle formation aims at quantifying the final result of a specific laser-ionized volume in the cloud chamber. It therefore provides a lower limit to the actual formation rates, since particle losses, e.g. due to self-coagulation or wall losses, directly impact the calculated

value. Furthermore, the calculation rates per unit plasma volume do not imply that particles are actually produced within the filament volume itself. They can also be produced in the subsequent evolution of the atmosphere around the filaments, depending on the diffusion of the produced species, as well as their dilution by the mixing fan. While allowing comparisons among the present study, in which all experiments were performed using the same experimental configuration, these limitations should be kept in mind when comparing our data with other experimental arrangements.

We recorded the light scattering by micrometric particles by using a 488 nm semiconductor laser (Coherent) directed horizontally through the AIDA chamber (Möhler et al., 2003; Schnaiter et al., 2012) in the near-forward direction, at a scattering angle of 2°. Cloud particles (supercooled droplets and/or ice crystals) are counted and sized by two optical particle counters (OPC, WELAS2000, Palas) in the respective size ranges of 0.7–46 μm (hereafter denoted OPC1) and 5.0–240 μm (OPC2).
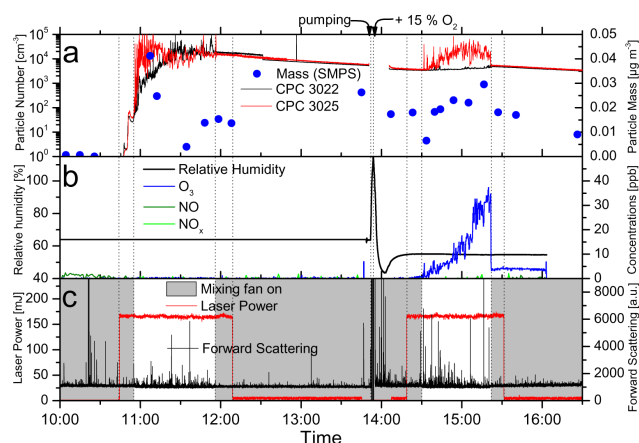
Fig. 2. Particle and trace gas formation by laser filaments for experiments 1 & 2 in pure argon and in an argon–oxygen mixture (15 % O_2) at 283 K and at 64 % as well as 55 % relative humidity, respectively. The panels show **(a)** aerosol particle number (black and red lines) and mass concentrations (blue circles); **(b)** relative humidity (black line), ozone (blue line), NO (dark green line), and NO_x concentrations (light green line); **(c)** as well as near-forward scattering (black line), laser power (red line) and mixing fan operation (shaded grey area). Dashed vertical lines indicate the time of events like switching on/off the laser, the fan, or a pump.

3 Results and discussion

In this section we will present and discuss the laser-induced particle formation in atmospheres composed of different main components and trace gases in the order of increasing complexity. We will start with pure humid argon, humid argon–oxygen mixtures, and humid nitrogen and will compare these results with experiments in humid synthetic air. In the following we will demonstrate the potential influence of different trace gases and particles on laser-induced particle formation. These results will then be compared with those obtained in humid ambient air. Finally, we will discuss the cloud activation of the laser-generated particles including growth of the nucleated particles.

3.1 Plasma-induced particle formation in humid argon, humid argon–oxygen mixtures, and humid nitrogen

We investigated laser-induced particle formation in an atmosphere consisting only of the noble gas argon and water vapour. In a second experiment 15 % of the argon was replaced by oxygen. We then repeated the experiment also in humid nitrogen.

3.1.1 Humid argon and humid argon/oxygen atmosphere

In pure humid argon the laser generated the brightest plasma of all experiments described in this paper. Figure 2 shows the evolution of particle number and mass, relative humid-
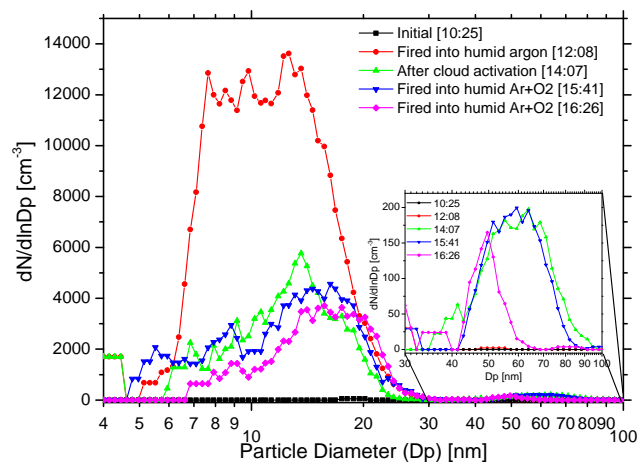

Fig. 3. Particle size distributions for selected times during experiments 1 & 2 in pure argon and in an argon–oxygen mixture (15 % O_2) at 283 K and at 64 % as well as 55 % relative humidity, respectively. Times in the legend refer to Fig. 2.

ity and trace gas mixing ratios, forward scattering intensity, laser power and mixing fan operation in three panels. Figure 3 shows particle size (D_p) distributions for different times during the experiment.

The first laser firing period starting at 10:44 CEST and lasting for 85 min was in humid argon only. The laser generates particles with diameters of 6 to 20 nm with a concentration of about $2 \times 10^4 \, \mathrm{cm}^{-3}$ in the 84.5 m^3 AIDA volume. The particles are produced at an effective rate of $4 \times 10^9 \, \mathrm{cm}^{-3}$ plasma s^{-1}. This rate is about 10 times higher than in pure synthetic air with similar water content as will be shown in Sect. 3.2. However, the total condensed mass is limited to below ~ 20 $\mathrm{ng\,m}^{-3}$, similar as in air (Fig. 2a). The particle mass is calculated from the measured size distributions assuming spherical particles and a density of 1.0 $\mathrm{g\,cm}^{-3}$. Note that the particle production is only visible during the periods when the laser was firing and the mixing fan was not diluting the plasma (cf. Sect. 3.1.2.). The particle number concentration measured by CPC3025 is more sensitive to the smaller freshly formed particles than that measured by CPC3022 and shows therefore higher concentrations especially when new particles are formed and the mixing fan is off. The forward scattering intensity of the 488 nm laser near the filaments shows some increased scatter but no significant increase during the formation of the relatively large number of new particles most likely due to their small diameter (Fig. 2c).

At 13:52, 155 hPa of the argon were pumped off and replaced by oxygen. The adiabatic expansion leads to a temporary drop in temperature from 283.6 to 272.4 K and a corresponding increase in relative humidity from 64 to 115 %. This supersaturation activated the existing aerosol particles to cloud droplets. After evaporation of the cloud droplets, aerosol particles of about 60 nm diameter were observed (see enlarged plot for this size range in Fig. 3). These particles
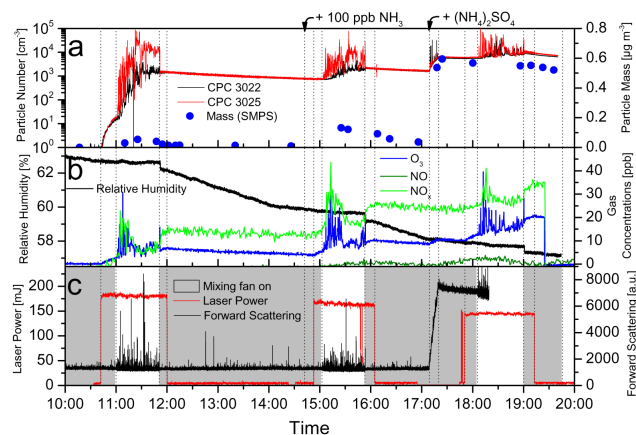
Fig. 4. Particle and trace gas formation by laser filaments in the synthetic air for experiments 4, 6, and 7 at 283 K and ∼ 60 % RH. The different panels show **(a)** particle number (red and black lines) and mass (blue circles); **(b)** relative humidity (black line), ozone (blue line, NO (dark green line) and NOₓ concentrations (light green line); **(c)** near-forward scattering (black line), laser power (red line) and mixing fan operation (grey shaded area).

Fig. 5. Particle size distributions for selected times during experiments 4, 6, and 7 in synthetic air at 283 K and about 60 % relative humidity. Times in the legend refer to Fig. 4.

were formed in the dense droplet cloud (e.g. by scavenging processes and not by the laser activity).

At 14:19 the laser started firing for 72 min into the humid argon–oxygen mixture. The particle number increased only slightly, and no significant increase in particle mass was observed. Only the ozone concentration increased substantially as could be expected from previous measurements (Petit et al., 2010) (Fig. 2b). The particle production is an order of magnitude reduced compared to pure argon. This may partly be due to the decrease of the relative humidity from 64 to 55 % due to the dilution of the moisture by the oxygen injected into the chamber. The reduction in particle production rate by the addition of 15 % of oxygen in the argon atmosphere from 4×10^9 to 4×10^8 cm^{-3} plasma s^{-1} is unlikely to stem from a lower plasma density, since the filament clamping intensity (Kasparian et al., 2000; Becker et al., 2001) is similar in both gases. Rather, the electron scavenging effect of O$_2$, or its capacity to generate ozone, may play an important role.

The persistence of new particle formation in argon atmospheres free of elemental nitrogen shows that nitric acid aerosol formation (Henin et al., 2011; Rohwetter et al., 2011) is not the exclusive process that can lead to formation of new particles. As there exist no low vapour pressure species containing just the elements hydrogen, oxygen and argon as present in these experiments, we conclude that the observed particles are related to contaminants in the chamber.

Although the contaminants are not identified and their concentration is unknown, we may roughly evaluate their influence by assuming a contamination of 0.1 ppm of hydrocarbons in the argon, i.e. the upper limit given by Air Liquide. Its complete oxidation in or near the laser-generated plasma
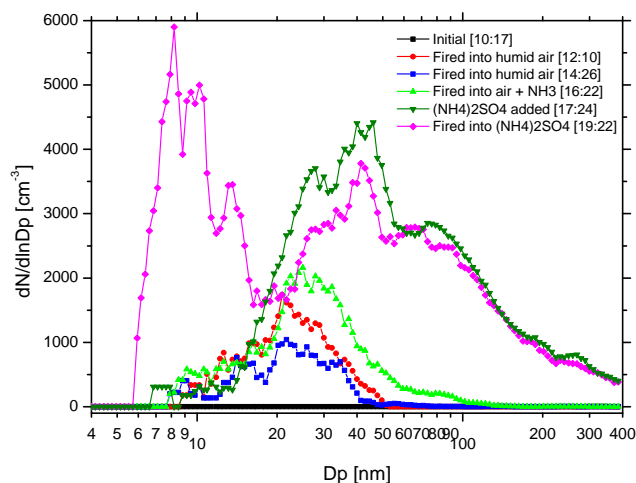
could potentially lead to formation of about 100 µg m^{-3} of particle mass. This is based on the estimate that 1 ppb of volatile organic hydrocarbon can form 1 µg m^{-3} of particle mass. Considering that every laser pulse (10 Hz) generates a new plasma volume of 0.08 cm^3, about 2880 cm^3 of the chamber volume of 84.5 m^3 (3.4×10^{-5}) are processed within one hour. This would correspond to a particle mass formation of a few ng m^{-3} h^{-1}, hence only about a factor of 5 less than the observations. Considering the uncertainties in these estimates and the possibility of additional contamination from the chamber walls, the majority of the particles observed in these experiments may indeed stem from laser-induced oxidation of background volatile organic compound (VOC) in the simulation chamber. The uncertainties about the potential contaminants are of course a limiting factor for the quantitative reproducibility of our experiments, for example, in other experiments.

3.1.2 Diluting the laser plasma with a fan

During periods when the mixing fan was switched off, strong local variations (e.g. like moving plumes) of trace gases and particles with high peak concentrations are observed (Figs. 2 and 4). Turning on the mixing fan leads to homogeneous concentrations throughout the whole chamber within about 1 min. Therefore, the amount of trace gases or particles formed by the laser plasma can only be quantified in the periods with the fan operating. Diluting the laser-generated plasma by using a mixing fan may be compared to atmospheric situations with a similar wind speed of about 1.5 m s^{-1}. The dilution does not prevent the formation of active species like ozone and NOₓ (cf. panel b in Figs. 2 (15:25) and 4 (e.g. 10:50)). Their concentrations continue to rise as long as the laser is active no matter if the fan is operating
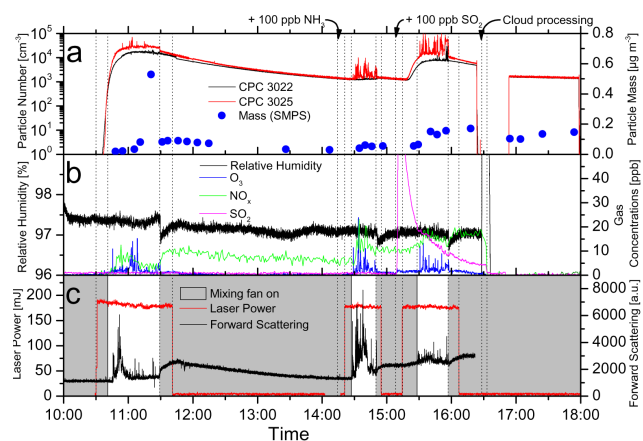
Fig. 6. Particle and trace gas formation by laser filaments in the synthetic air for experiments 5 and 8 at 283 K and 97 % RH. The panels show **(a)** particle number (red and black line) and mass (blue circles); **(b)** relative humidity (black line), ozone (blue line), NO_x (green line), and SO_2 concentrations (magenta line); **(c)** near-forward scattering (black line), laser power (red line) and mixing fan operation (grey shaded area).

Fig. 7. Particle size distributions for selected times during experiments 5 and 8 in synthetic air at 283 K and about 97 % relative humidity. Times in the legend refer to Fig. 6.

or not. In contrast, new particle formation stops or reduces substantially when the fan dilutes the plasma in both the weak and the strong filamentation regimes. This is visible, for example, in Fig. 9a at 11:55 for weak filamentation and in Figs. 2a and 4a (at 10:50 for both) for strong filamentation. Dilution of the plasma obviously reduces local concentrations of active species (e.g. radicals, atoms, ions), hence reducing reaction rates for formation of condensable molecules available for nucleation of new particles. For these relatively clean conditions in terms of trace gas concentrations, already dilution simulating a moderate wind speed is sufficient to efficiently suppress new particle formation. This is different when additional trace gases are present or for typical ambient air as will be shown in Sects. 3.3 and 3.4.

3.1.3 Humid nitrogen atmosphere

In a humid nitrogen atmosphere (74 % RH) in the weak filamentation regime, particle production rates were similar to those in humid argon with strong filamentation. Furthermore, 10–20 ppb of NO and NO_x were generated. The particles that were formed by the laser filaments were smaller than 30 nm in diameter. The relatively high particle production rate despite the weak filamentation may be caused by formation of nitric acid (Henin et al., 2011), a pathway not open in experiments 1 and 2 (Dotan et al., 1997; Bradsley, 1968), as discussed in Sect. 3.1.1. In the humid nitrogen atmosphere, NO and NO_x are most probably produced without ozone as intermediate using the oxygen atoms provided by water molecules. This finding illustrates the need to identify other oxidation channels, based e.g. on the OH radicals, as well as ions and excited species produced in the filament plasma.
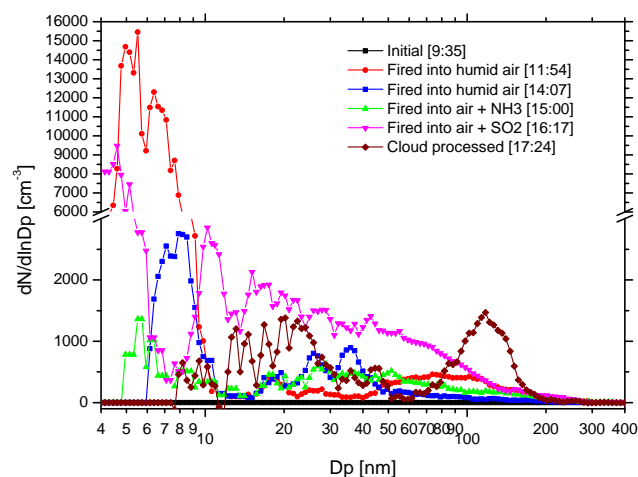
3.2 Humid synthetic air atmosphere

Laser-induced particle and trace gas generation in humid synthetic air will be described in this section as well as the influence of the water concentration.

3.2.1 Particle and trace gas formation

Particle and trace gas formation was studied in humid synthetic air for relative humidities ranging from 25 to 99 % at 283 K. Illuminating the chamber atmosphere with laser filaments results in the formation of NO_x, ozone and nanometer-scale particles from a low background atmosphere. Two representative experiments are shown for relative humidities of $\sim 60\%$ (Figs. 4 and 5) and 97 % (Figs. 6 and 7), respectively.

Generating laser plasma for 78 min in AIDA with the mixing fan switched off for 51 min led to the formation of 7 ppb of ozone, 13 ppb of NO_x, and $\sim 1200\,cm^{-3}$ new particles of 18 nm geometric mean diameter (GMD) and a geometric standard deviation (GSD) of 1.8. These particles were stable at 283 K and 62 % relative humidity in AIDA, and the integrated mass concentration amounted to about 15 ng m^{-3}. The particle formation rate was $3.2 \times 10^8\,cm^{-3}$ plasma s^{-1}, about an order of magnitude smaller than those observed in pure argon with 64 % relative humidity. In a similar experiment (laser plasma for 70 min with 48 min fan off) at 97 % relative humidity, 2 ppb of ozone, 10 ppb of NO_x, and two separated modes of particles were formed, one with about $16\,000\,cm^{-3}$ very small particles (~ 6 nm GMD, 1.3 GSD) and one with about $2000\,cm^{-3}$ larger particles with a GMD of 101 nm and a GSD of 1.6. This large concentration of new particles induced a significant increase of the forward scattering signal intensity (cf. Fig. 6c), which was not the case in the experiment at $\sim 60\%$ relative humidity (cf. Fig. 4c). The larger particles formed at 97 % relative humidity seemed
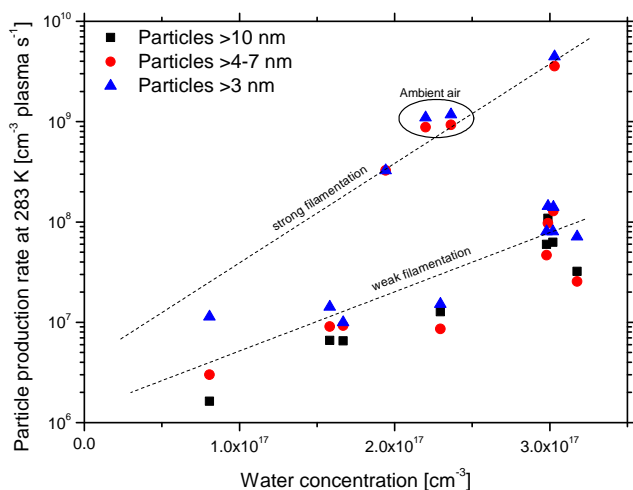
Fig. 8. Formation rates for particles of different sizes in the laser plasma in humid synthetic air at 283 K for water concentrations between 8×10^{16} and 3×10^{17} cm^{-3}. Two experiments with ambient air (cf. Sect. 3.4) are added for comparison. Dashed lines are just to guide the eyes to the results for pure humid air for the two filamentation regimes.

to be less stable than the small ones, which is reflected in a relative fast decrease of the integrated particle mass concentration from initially 90 to 35 ng m^{-3} over two hours (cf. Fig. 6a). In the experiment with higher humidity, significantly less ozone but similar amounts of NO$_x$ were formed. The particle formation rate was 4.4×10^9 cm^{-3} plasma s^{-1}, about an order of magnitude higher than in synthetic air with 62 % RH but comparable to those observed in pure argon with 64 % relative humidity. The observed differences in particle mass and number are not yet fully understood but may be influenced by the different amounts of water vapour with the higher water concentration favouring the particle formation, e.g. by higher OH radical yields in the plasma (Fresnet et al., 2002; Gordillo-Vásquez and Donkó, 2009). Furthermore, if the newly formed particles consisted of mainly inorganic molecules like HNO$_3$, their volume would triple and the diameter would double by water uptake when changing the relative humidity from 60 to 97 % (according to the Aerosol Inorganics Model (AIM)(Wexler and Clegg, 2002)). Besides such reasons for the observed differences in the two experiments, the possibility exists that also changing background contaminations of a few ppb of VOCs, which cannot be excluded for these experiments, might have caused them. New nano-size particles were always formed in the AIDA simulation chamber as long as the mixing fan was switched off. In contrast, new particle formation shown in Figs. 4 and 6 is very weak when the laser is turned on and the mixing fan is still working (cf. Sect. 3.1.2). Only when the mixing fan is turned off, the laser-induced particle formation becomes significant.

3.2.2 Influence of humidity on new particle formation

The laser plasma-induced particle formation in humid synthetic air is a strong, almost exponential function of the water concentration as shown in Fig. 8 for both filamentation regimes. Note that the scatter in the data stems predominantly from fluctuations in the laser filament intensity, although also variations in the background contamination of the chamber may have an impact. Despite the scatter in the individual data points, the particle formation rate ranges from a few 10^6 cm^{-3} plasma s^{-1} for weak filamentation up to 5×10^9 cm^{-3} plasma s^{-1} for strong filamentation for water molecule concentrations between 8×10^{16} and 3.2×10^{17} cm^{-3} corresponding to relative humidities between 25 and 98 % at 283 K. The abundance of water vapour obviously plays an important role for the generation of reactive species, e.g. ions and radicals (Fresnet et al., 2002; Gordillo-Vásquez and Donkó, 2009) in the laser plasma, and therefore can strongly influence the particle formation rates.

Experiments in humid argon and nitrogen show enhanced particle production rates as compared to humid air for similar water concentrations (cf. Table 1). The ambient air experiment, which will be described in Sect. 3.4, seems to be in line with those in synthetic air done also in the strong filamentation regime. Laser power and the corresponding strong or weak filamentation, as well as the water content, control the particle production within the laser plasma. Despite the exponential increase of the particle formation rate with water concentration, the influence of other trace gases can be even higher. Although we have no evidence that our purified water (Barnstead Nanopure) contains significant amounts of impurities, we can not exclude them on a ~ 50 ppt level, which could potentially impact nucleation. However, experiments with ambient air with no additional water added to the chamber seem to be in line with the water dependence of the particle production observed in humidified synthetic air (Fig. 8). This provides an indication that the interaction of active species (e.g. OH radicals) generated in the plasma and depending on water concentration, rather than impurities in the nanopure water, promotes particle formation.

3.3 Influence of trace gases and background particles in humid synthetic air

3.3.1 NH$_3$ and ammonium sulfate background aerosol

NH$_3$ is known to strongly influence particle nucleation (Kirkby et al., 2011), e.g. by stabilizing acidic clusters, and may act as a scavenger of labile photoproducts from the laser plasma. Indeed in the presence of 100 ppb of ammonia (see Fig. 4 – 15:00, 60 % relative humidity), the increases in particle size (up to 100 nm) and mass are larger than in the previous run without ammonia. However, under these conditions, NH$_3$ appears to have no significant influence on the laser-induced particle production rate or the formation of
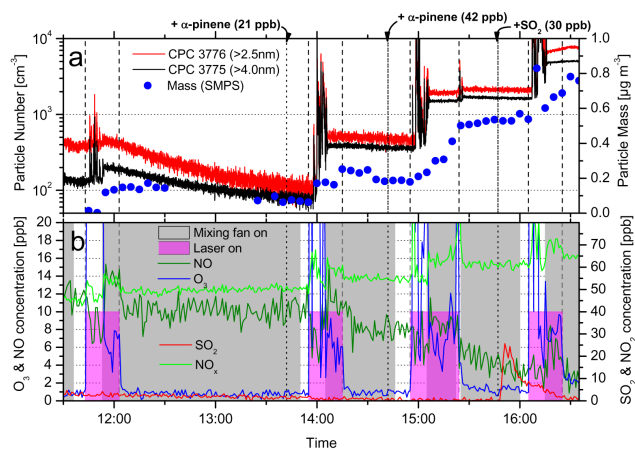
Fig. 9. Laser-induced particle formation in the presence of α-pinene and SO_2 at 283 K and a relative humidity decreasing from 94 to 89 %, **(a)** evolution of particle number (red and black line) and mass (blue circles); **(b)** evolution of NO (dark green line), NO_x (light green line), O_3 (blue line), SO_2 (red line) mixing ratios and operation of fan (grey shaded area) and laser (pink area, 140 mJ).

Fig. 10. Evolution of particle sizes for laser-induced particle formation in humid synthetic air in the presence of α-pinene and SO_2 at 283 K and 94–89 % relative humidity. Times in the legend correspond to Fig. 9.

ozone and NO_x. For the experiment at 97 % relative humidity (see Fig. 6 – 14:30, 97 % relative humidity), the addition of 100 ppb NH_3 did not increase the particle production rate and had no significant effect on size and mass of the formed particles or the amounts of ozone and NO_x. Probably the effects of the higher water concentration (see Sect. 3.2.2.) mask the potential changes due to the presence of ammonia in this case.

In the experiment presented in Fig. 4 (see 17:10, 60 % relative humidity) 4800 cm^{-3} $(NH_4)_2SO_4$ aerosol particles with a broad size distribution peaking at 80 nm were added to the AIDA chamber corresponding to a total mass of 1 µg m^{-3} to represent typical background atmospheric aerosol. With the laser plasma, 4000–5000 cm^{-3} new particles with a GMD of 10 nm were produced, which then coagulated predominantly with the larger particles. The new particles may be formed by evaporation of the $(NH_4)_2SO_4$ particles present in the plasma beam and subsequent nucleation of sulfate-containing particles in the diluting plasma. As in the previous experiments, also this new particle formation is suppressed almost completely by enhanced dilution of the filaments with the mixing fan (see Sect. 3.1.2.).

3.3.2 SO_2

To gain an insight into the mechanism of laser-induced formation of nanometric particles, we also investigated the influence of SO_2 (cf. Fig. 6). Firing the laser in a synthetic air atmosphere at 283 K and 51 % relative humidity with 10–20 ppb of SO_2 resulted in an increase of the particle production rate by two orders of magnitude to 1.8×10^9 cm^{-3} plasma s^{-1}, as compared with the laser effect in an SO_2-free atmosphere for weak filamentation. For strong filamentation, the particle formation rates in air and air + SO_2 are in
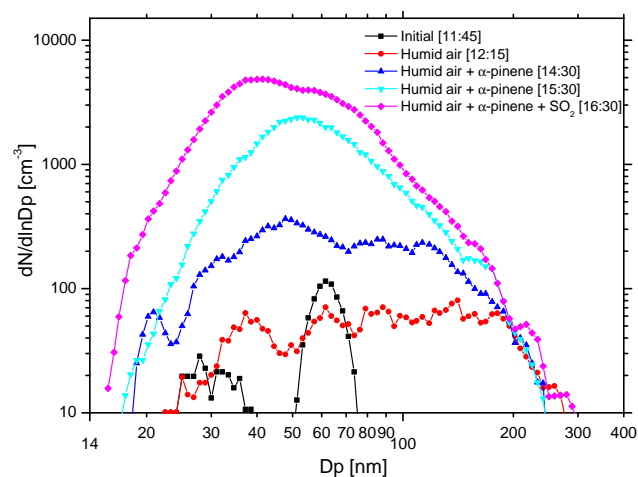
the same range of, for example, 2.4×10^9 cm^{-3} plasma s^{-1} (cf. Fig. 6, 15:15). The behaviour of the particles formed in a SO_2-doped atmosphere illustrates the difference in the processes leading to particle formation on one side, and their growth on the other side. While in presence of about 10 ppb SO_2 the particle production rate increases drastically, the particles stay mostly below 20 nm and the particle mass increase is not significantly enhanced. In an experiment at 97 % relative humidity, elevated ammonia concentrations, and SO_2 decreasing from 60 down to 7 ppb the particle formation started already in the phase when the mixing fan was still in operation (see Fig. 6a). In the presence of SO_2, the plasma always generated a large number of particles in the size range below 20 nm, as can be seen exemplarily in Fig. 7 (16:17), where also the number of larger particles increased significantly. The particle volume formed in this experiment after processing of SO_2 is consistent with a sulfate mass load of (0.28 ± 0.14)µg m^{-3} obtained from filter sample analysis by ion chromatography considering that in Fig. 6a a nominal density of 1.0 g cm^{-3} was used. This is consistent with the measurement of the dry size distribution and would correspond to a conversion of about 70 ppt of SO_2 into sulfuric acid in and near the plasma region leading to formation of sulfate particles. The contribution SO_2 from beyond the filament volume itself is evidenced by considering that, operating for 52 min at 10 Hz, the laser filaments process only about 2496 cm^3 of the chamber volume of 84.5 m^3 (2.95×10^{-5}). With an average SO_2 concentration of 30 ppb, this would lead to conversion of only 0.9 ppt of SO_2. Hence, the actual conversion of SO_2 into sulfate is about two orders of magnitude more efficient than obtained from this rough estimate. Most of the SO_2 must therefore be oxidized by reactive species that are produced in the filament and subsequently
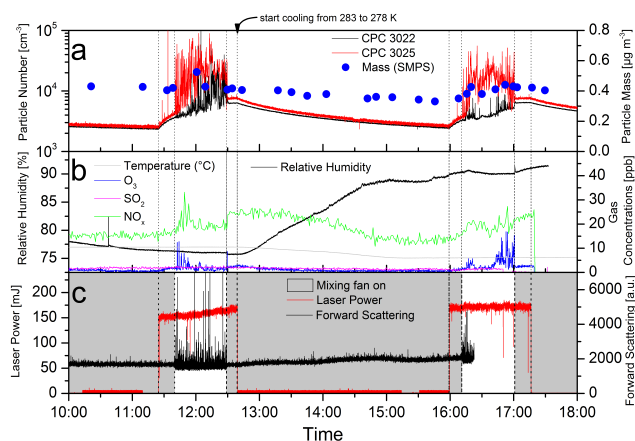
Fig. 11. Particle and trace gas formation by laser filaments in ambient air at 283.6 K and ∼ 76 % RH and 279 K and ∼ 90 % RH. The panels show **(a)** particle number (red and black line) and mass (blue circles); **(b)** relative humidity (black line), ozone (blue line), SO_2 (pink line), and NO_x (green line) concentrations; **(c)** near-forward scattering (black line), laser power (red line) and mixing fan operation (grey shaded area).
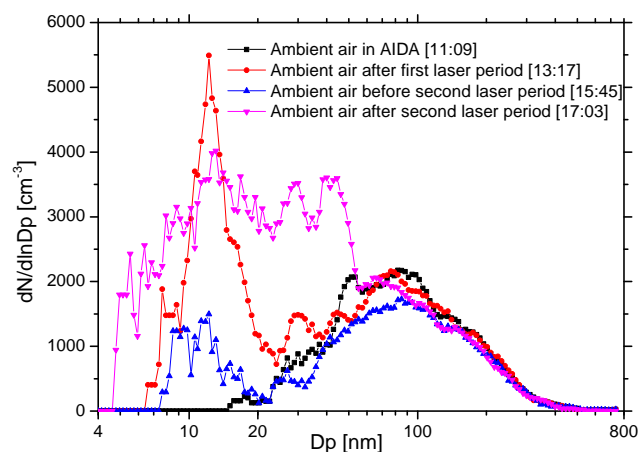

Fig. 12. Particle size distributions for selected times during the experiment with laser filaments in ambient air in the AIDA simulation chamber at 283.6 K and ∼ 76 % RH and 279 K and ∼ 90 % RH. Times in the legend correspond to Fig. 11.

dispersed around them by transport and diffusion. A more detailed quantification is however hindered by the limited knowledge about the plasma region and especially the distribution of reactive species like the OH radicals.

3.3.3 Toluene and α-pinene

In presence of 22 ppb of toluene at 245 K and 88 % relative humidity, no significant additional particle mass was formed when the laser fired. Only the particle production rate increased in the weak filamentation regime by a factor of ∼ 6 from 2.8×10^7 cm^{-3} plasma s^{-1} without toluene to 1.6×10^8 cm^{-3} plasma s^{-1}. This is probably not only caused by negligible reactivity of toluene towards ozone that is formed in the plasma but also by its limited ability to form condensable products in reaction with the active plasma species.

These results are in strong contrast to those obtained for the biogenic hydrocarbon α-pinene at 283 K. In presence of 21 ppb (124 µg m^{-3}) and 63 ppb (370 µg m^{-3}) of the unsaturated terpene α-pinene, the particle production rate increases for the weak filamentation regime from 1.4×10^8 cm^{-3} plasma s^{-1} before adding the VOC to 3.6×10^8 and 1.0×10^9 cm^{-3} plasma s^{-1}, respectively (Fig. 9). As observed in absence of VOCs, the increase in particle number is further enhanced by the subsequent injection of SO_2 in the chamber. α-Pinene does not only assist new particle formation, but also increases the particle size (up to 200 nm) resulting from a larger condensable mass. The corresponding particle volume rises up to 0.2×10^{-6} cm^3 m^{-3} and 0.5×10^{-6} (corresponding to 0.2 and 0.5 µg m^{-3} assuming a density of 1.0 g cm^{-3}), condensing about 0.16 and 0.14 % of the total

available VOC mass of 124 and 370 µg m^{-3}, respectively. In case of the unsaturated α-pinene, the particle formation proceeds also via its oxidation by the ozone that is formed in the filaments. Therefore, α-pinene can promote particle formation also when the laser is not operating, but sufficient amounts of ozone are present. The resulting oxidized species, most probably organic acids, nucleate new particles. This observation evidences the importance of ozone as an intermediate product in the reaction for secondary particle formation. Laser-generated ozone will of course always react with α-pinene, which can also lead to new particle formation if the VOC and ozone concentrations are high enough.

In another experiment with synthetic air at 283 K and 89 % relative humidity, 30 ppb of SO_2 were added to the α-pinene level of about 63 ppb. When the laser fired, 7 ppb of SO_2 were still present and the particle production rate was 4.8×10^9 cm^{-3} plasma s^{-1}, a factor of five higher compared to the gas mixture without SO_2. The increase rate in particle mass however did not change significantly. This is also visible in Figs. 9 and 10 by the large number of small particles formed in the presence of SO_2.

3.4 Humid ambient air

To investigate the effect of the laser-induced plasma in ambient air, we filled the simulation chamber in the morning of 21 October 2011 with ambient air only removing particles larger than 10 µm by a PM_{10} inlet. With the ambient air in the chamber at 283.6 K, a relative humidity of 79–76 % was reached. After the first experiment the chamber was cooled with 3 K h^{-1} to 279 K increasing the relative humidity to ∼ 90 % for another experiment. The ambient air contained insignificant amounts of ozone (< 2 ppb) and SO_2 (< 2 ppb) but about 15 ppb of NO_x and 2800 cm^{-3} particles (Fig. 11) with a size distribution representing the accumulation mode

size range (20–400 nm) with a GMD of 90 nm and a GSD of 1.8 as shown in Fig. 12. Analysis of filter samples resulted in a sulfate concentration of $(1.2 \pm 0.6) \, \mu g \, m^{-3}$, which is more than the mass of $0.7 \, \mu g m^{-3}$ calculated from the integrated size distribution using a density of $1.77 \, g \, cm^{-3}$ of $(NH_4)_2SO_4$. This may be explained by a small number of sulfate-containing particles larger than the upper end of the measurement range of the scanning mobility particle sizer of 736 nm.

In contrast to most previous experiments, at $\sim 76\%$ relative humidity and 283 K, substantial laser-induced particle formation occurred in ambient air even with mixing fan in operation. The particle production rate was $1.1 \times 10^9 \, cm^{-3}$ plasma s^{-1}. The new particles had a peak diameter of 12 nm. Switching off the mixing fan did not significantly change the particle production rate. At $\sim 90\%$ relative humidity and 279 K, no significant change of the particle production rate compared to the run at $\sim 76\%$ relative humidity could be observed. However, in contrast to the previous run, the particles formed were larger with diameters of up to 70 nm, and an increase of particle mass by about $0.1 \, \mu g \, m^{-3}$ could be detected (cf. Fig. 11).

The minimal influence of the mixing fan on particle production can be understood by considering that, contrary to synthetic air where the laser has to produce all reagents implied in the particle formation process, the ambient air contains numerous trace gases already in appreciable concentrations, homogeneously spread in the whole chamber. Therefore, diluting the filament volume is less critical for the formation of condensable species.

3.5 Cloud processing of laser-generated particles

In several experiments in the temperature range between 283 and 245 K, the laser plasma-generated particles were activated by adiabatic expansion in the AIDA chamber to form water clouds (Wagner et al., 2006). In all cases most of the particles nucleated water close to water saturation as typical for soluble species. For two different experiments the particle size distributions before and after such cloud processing at 283 K are shown. Figure 3 (14:07) shows an example for particles generated in pure argon and growing to a mode size of about 60 nm by single cloud activation. Figure 7 shows this for a sulfate-containing aerosol that forms a particle mode with a size of 120 nm by cloud processing (see size distribution for 17:24). Since the particle mass concentrations do not increase by cloud processing, the observed increase in particle size may be caused by scavenging of the possibly highly charged aerosol particles by the cloud droplets leading to larger particles once the cloud droplets have lost their water.

Considering the increasing particle formation rates with increasing water concentration or relative humidity, one might wonder if the particle production rates were higher for supersaturated conditions. So far we have not found sig-

nificant evidence for this. Furthermore, generating laser filaments in simulated droplet clouds did not seem to significantly change the properties of these clouds. More details of the influence of laser filaments on ice clouds at much lower temperatures will be discussed in a separate paper (Duft et al., 2013).

4 Conclusions

Under controlled simulated atmospheric conditions, and especially low background particle concentrations ($\leq 0.1 \, cm^{-3}$), terawatt laser plasma filaments generated new particles that grew to sizes of 3 to 130 nm during the experiment. In weakly polluted ambient air in the simulation chamber, production rates range up to the order of $1 \times 10^9 \, cm^{-3}$ plasma s^{-1}. Although these rates depend on the actual experimental conditions, we may note that it lies 5–6 orders of magnitude above the 10^4–$10^5 \, cm^{-3} \, s^{-1}$ observed in coastal areas and industrial plumes (Kulmala et al., 2004), but of course limited to the filament volume.

The new particle formation occurs even in humid inert gas atmospheres in which it is most likely driven by the inevitable presence of lower ppb levels of volatile organic trace contaminants. Adding oxygen to the inert gas reduced the particle production rate by an order of magnitude, which is consistent with the high electron scavenging efficiency of oxygen, reducing the plasma reactivity. In the presence of humid nitrogen, the particle production rates are not significantly enhanced compared to humid argon, although the formation of inorganic species like HNO_3 would be possible. In synthetic air, the particle production rate is comparable to that of an argon/oxygen mixture, indicating that nitrogen chemistry (e.g. via HNO_3) is not the exclusive process for particle production. The new particle formation in synthetic air shows an exponential increase with the water concentration. This points to the important role water molecules play in the formation of clusters (Kurtén et al., 2007) and underlines the relevance of the water molecules for the formation of reactive species like OH radicals in the plasma, which have the ability to generate condensable species like inorganic acids or oxidized organic molecules (Henin et al., 2011; Fresnet et al., 2002). Without additional trace gases added, the typical particle diameters generated range between 5 and 20 nm. At 97% relative humidity and 283 K, also surprisingly large particles with a diameter of about 100 nm could be observed. As expected, the formation and growth of new particles is significantly promoted in the presence of trace gases like NH_3, SO_2 or volatile organics like toluene or α-pinene. While SO_2 strongly supports the formation of small particles with limited impact on particle mass, organic species like α-pinene have a major impact on particle growth. This different behaviour underlines that several pathways contribute to laser-induced new particle formation and growth: understanding and quantifying the full physico-chemistry of the laser effect

will require extensive experimental and modelling work well beyond the scope of the present paper.

The particles remained relatively small at 76 % relative humidity and only grew into the accumulation mode size range for a relative humidity of 90 %. Under these conditions an increase in particle mass by 30 % was also detectable. Particle production rates were similar to experiments with pure synthetic air at 97 % relative humidity, although it contained initially no particles and trace gases. With ambient air in the simulation chamber, the dilution of the laser plasma had no significant influence on the new particle formation, in contrast to most other experimental conditions reported in this work in which dilution suppressed the laser-induced particle formation. Considering a potential impact of the laser-generated particles on clouds, we conclude that these particles nucleate water close to water saturation as typical for soluble species.

Edited by: A. Kiendler-Scharr

References

Bardsley, J. N.: The theory of dissociative recombination, J. Phys. B, 1, 365–380, 1968.

Becker, A., Aközbek, N., Vijayalakshmi, K., Oral, E., Bowden, C. M., and Chin, S. L.: Intensity clamping and re-focusing of intense femtosecond laser pulses in nitrogen molecular gas, Appl. Phys. B, 73, 287–290, 2001.

Béjot, P., Kasparian, J., Henin, S., Loriot, V., Vieillard, T., Hertz, E., Faucher, O., Lavorel, B., and Wolf, J.-P.: Higher-order Kerr terms allow ionization-free filamentation in gases, Phys. Rev. Lett., 104, 103903, doi:10.1103/PhysRevLett.104.103903, 2010.

Bergé, L., Skupin, S., Nuter, R., Kasparian, J., and Wolf, J.-P.: Ultra-short filaments of light in weakly-ionized, optically-transparent media, Rep. Prog. Phys., 70, 1633–1713, doi:10.1088/0034-4885/70/10/R03, 2007.

Braginskiy, O. V., Vasilieva, A. N., Klopovskiy, K. S., Kovalev, A. S., Lopaev, D. V., Proshina, O. V., Rakhimova, T. V., and Rakhimov, A. T.: Singlet oxygen generation in O_2 flow excited by RF discharge: II. Inhomogeneous discharge mode: plasma jet, J. Phys. D: Appl. Phys., 38, 3609–3625, 2005.

Chin, S. L., Hosseini, S. A., Liu, W., Luo, Q., Théberge, F., Aközbek, N., Becker, A., Kandidov, V. P., Kosareva, O. G., and Schröder, H.: The propagation of powerful femtosecond laser pulses in optical media: physics, applications, and new challenges, Can. J. Phys., 83, 863–905, 2005.

Couairon, A. and Mysyrowicz, A.: Femtosecond filamentation in transparent media, Phys. Rep., 44, 47–189, 2007.

Dotan, I., Hierl, P. M., Morris, R. A., and Viggiano, A. A.: Rate constants for the reactions of N^+ and N_2^+ with O_2 as a function of temperature (300–1800 K), Int. J. Mass Spectrom. Ion Process., 167/168, 223–230, 1997.

Duft, D., Möhler, O., Saathoff, H., Schnaiter, M., Leisner, T., Henin, S., Stelmaszczyk, K., Petrarca, M., Delagrange, R., Hao, Z. Q., Lüder, J., Petit, Y., Rohwetter, P., Kasparian, J., Wolf, J.-P., and Wöste, L.: Laser filament induced ice mulitplication under cirrus cloud conditions, Proc. Natl. Acad. Sci., submitted, 2013.

Fresnet, F., Baravian, G., Magne, L., Pasquiers, S., Postel, C., Puech, V., and Rousseau, A.: Influence of water on NO removal by pulsed discharge in $N_2/H_2O/NO$ mixtures, Plasma Sources Sci. Technol., 11, 152–160, 2002.

Gordillo-Vásquez, F. J. and Donkó, Z.: Electron energy distribution functions and transport coefficients relevant for air plasmas in the troposphere: impact of humidity and gas temperature, Plasma Sources Sci. Technol., 18, 034021, doi:10.1088/0963-0252/18/3/034021, 2009.

Henin, S., Petit, Y., Rohwetter, P., Stelmaszczyk, K., Hao, Z. Q., Nakaema, W. M., Vogel, A., Pohl, T., Schneider, F., Kasparian, J., Weber, K., Wöste, L., and Wolf, J.-P.: Field measurements reveal mechanism of laser-assisted water condensation, Nat. Commun., 2, 456, doi:10.1038/ncomms1462, 2011.

Ju, J., Liu, J., Wang, C., Sun, H., Wang, W., Ge, X., Li, C., Chin, S. L., Li, R., and Xu, Z.: Laser-filamentation-induced condensation and snow formation in a cloud chamber, Opt. Lett., 37, 1214–1216, 2012.

Kasparian, J. and Wolf, J.-P.: Physics and applications of atmospheric nonlinear optics and filamentation, Opt. Express, 16, 466–493, 2008.

Kasparian, J., Sauerbrey, R., and Chin, S. L.: The critical laser intensity of self-guided light filaments in air, Appl. Phys. B, 71, 877–879, 2000.

Kasparian, J., Rodriguez, M., Méjean, G., Yu, J., Salmon, E., Wille, H., Bourayou, R., Frey, S., André, Y.-B., Mysyrowicz, A., Sauerbrey, R., Wolf, J.-P., and Wöste, L.: White-Light Filaments for Atmospheric Analysis, Science, 301, 61–64, 2003.

Kirkby, J., Curtius, J. Almeida, J., Dunne, E., Duplissy, J., Ehrhart, S., Franchin, A., Gagne, S., Ickes, L., Kurten, A., Kupc, A., Metzger, A., Riccobono, F., Rondo, L., Schobesberger, S., Tsagkogeorgas, G., Wimmer, D., Amorim, A., Bianchi, F., Breitenlechner, M., David, A., Dommen, J., Downard, A., Ehn, M., Flagan, R. C., Haider, S., Hansel, A., Hauser, D., Jud, W., Junninen, H., Kreissl, F., Laaksonen, A., Lehtipalo, K., Lima, J., Lovejoy, E.R., Makhmutov, V., Mathot, S., Mikkila, J., Minginette, P., Mogo, S., Nieminen, T., Onnela, A., Pereira, P., Petaja, T., Schnitzhofer, R., Seinfeld, J. H., Sipila, M., Stozhkov, Y., Stratmann, F., Tome, A., Vanhanen, J., Viisanen, Y., Vrtala, A., Wagner, P.E., Walther, H., Weingartner, E., Wex, H., Winkler, P. M., Carslaw, K. S., Worsnop, D. R., Baltensperger, U., and Kulmala, M.: Role of sulphuric acid, ammonia and galactic cosmic rays in atmospheric aerosol nucleation, Nature, 476, 429–433, 2011.

Kossyi, I. A., Kostinsky, A. Yu., Matveyev, A. A., and Silakov, V. P.: Kinetic scheme of the non-equilibrium discharge in

nitrogen-oxygen mixtures, Plasma Sources Sci. Technol., 1, 207–220, doi:10.1088/0963-0252/1/3/011, 1992.

Kulmala, M., Vehkamaki, H., Petäjä, T., Dal Maso, M., Lauri, A., Kerminen, V.-M., Birmili, W., and McMurry, P. H.: Formation and growth rates of ultrafine atmospheric particles: a review of observations, J. Aerosol Sci., 35, 143–176, 2004.

Kurtén, T., Torpo, L., Ding, C.-G., Vehkamäki, H., Sundberg, M. R., Laasonen, K., and Kulmala, M.: A density functional study on water-sulfuric acid-ammonia clusters and implications for atmospheric cluster formation, J. Geophys. Res., 112, D04210, doi:10.1029/2006JD007391, 2007.

Möhler, O., Stetzer, O., Schaefers, S., Linke, C., Schnaiter, M., Tiede, R., Saathoff, H., Krämer, M., Mangold, A., Budz, P., Zink, P., Schreiner, J., Mauersberger, K., Haag, W., Kärcher, B., and Schurath, U.: Experimental investigation of homogeneous freezing of sulphuric acid particles in the aerosol chamber AIDA, Atmos. Chem. Phys., 3, 211–223, doi:10.5194/acp-3-211-2003, 2003.

Petit, Y., Henin, S., Kasparian, J., and Wolf, J.-P.: Production of ozone and nitrogen oxides by laser filamentation, Appl. Phys. Lett., 97, 021108, doi:10.1063/1.3462937, 2010.

Rodriguez, M., Bourayou, R., Méjean, G., Kasparian, J., Yu, J., Salmon, E., Scholz, A., Stecklum, B., Eislöffel, J., Laux, U., Hatzes, A. P., Sauerbrey, R., Wöste, L., and Wolf, J.-P.: Kilometer-range non-linear propagation of femtosecond laser pulses, Phys. Rev. E, 69, 036607, doi:10.1103/PhysRevE.69.036607, 2004.

Rohwetter, P., Kasparian, J., Stelmaszczyk, K., Hao, Z., Henin, S., Lascoux, N., Nakaema, W. M., Petit, Y., Queißer, M., Salamé, R., Salmon, E., Wöste, L., and Wolf, J.-P.: Laser-induced water condensation in air, Nat. Photon., 4, 451–456, doi:10.1038/NPHOTON.2010.115, 2010.

Rohwetter, P., Kasparian, J., Wöste, L., and Wolf, J.-P.: Modelling of HNO_3-mediated laser-induced condensation: A parametric study, J. Chem. Phys., 135, 134703, doi:10.1063/1.3644591, 2011.

Schnaiter, M., Büttner, S., Möhler, O., Skrotzki, J., Vragel, M., and Wagner, R.: Influence of particle size and shape on the backscattering linear depolarisation ratio of small ice crystals – cloud chamber measurements in the context of contrail and cirrus microphysics, Atmos. Chem. Phys., 12, 10465–10484, doi:10.5194/acp-12-10465-2012, 2012.

Sorokin, A.: One conceivable mechanism of UV-light induced SO_2 Oxidation to H_2SO_4, Atmos. Chem. Phys., 10, 3141–3145, doi:10.5194/acp-10-3141-2010, 2010.

Sorokin, A. and Arnold, F.: Analysis of experiments on ion-induced nucleation and aerosol formation in the presence of UV light and ionizing radiation, Atmos. Environ., 43, 3799–3807, 2009.

Wagner, R., Bunz, H., Linke, C., Möhler, O., Naumann, K.-H., Saathoff, H., Schnaiter, M., and Schurath, U.: Chamber Simulations of Cloud Chemistry: The AIDA Chamber. Environmental Simulation Chambers: Application to Atmospheric Chemical Processes, NATO Science Series: IV: Earth Environmental Sciences, 62, 67–82, doi:10.1007/1-4020-4232-9_5, 2006.

Wexler, A. S. and Clegg, S. L: Atmospheric aerosol models for systems including the ions H^+, NH_4^+, Na^+, SO_4^{2-}, NO_3^-, Cl^-, Br^- and H_2O, J. Geophys. Res., 107, 4207, doi:10.1029/2001JD000451, 2002.

Wille, H., Rodriguez, M., Kasparian, J., Mondelain, D., Yu, J., Mysyrowicz, A., Sauerbrey, R., Wolf, J.-P., and Wöste, L.: Teramobile: a mobile femtosecond-terawatt laser and detection system, Eur. Phys. J.-Appl. Phys., 20, 183–190, 2002.

Xu, H. L., Azarm, A., Bernhardt, J., Kamali, Y., and Chin, S. L.: The mechanism of nitrogen fluorescence inside a femtosecond laser filament in air, Chem. Phys., 360, 171–175, doi:10.1016/j.chemphys.2009.05.001, 2009.

Yoshihara, K.: Laser-induced Mist and Particle Formation from Ambient Air, A Possible New Cloud Seeding Method, Chem. Lett., 34, 1370–1371, doi:10.1246/cl.2005.1370, 2005.